Reversal of Catalytic Material Substrate Selectivity through Partitioning of Polymers in Hierarchically Ordered Virus-Like Particle Frameworks

Pawel Kraj†, Nathasha D. Hewagama†, Byeongdu Lee‡, Trevor Douglas†*

† Department of Chemistry, Indiana University, 800 East Kirkwood Avenue, Bloomington, Indiana 47405, United States

‡ X-ray Science Division, Advanced Photon Source, Argonne National Laboratory, 9700 South Cass Avenue, Argonne, Illinois 60439, United States

*Corresponding Author trevdoug@indiana.edu

Abstract

Control over the selectivity of catalytic materials is a topic of growing interest. Virus-like particle (VLP) based materials such as protein macromolecular frameworks (PMFs) are promising for catalytic applications due to their ease of assembly, modular ability to encapsulate a variety of enzymes, and ease of separation from a reaction mixture. Here we demonstrate reversal of the initially negative material charge through the titration of a positively charged polymer into the material, causing the reversal of guest molecule uptake and enzymatic activity of PMFs. The charge-inverse material partitions a charged enzyme substrate to concentrate the substrate near an enzyme incorporated within the material, generating up to 5.9-fold increases in enzyme activity towards the partitioned substrate over the excluded substrate. We also show that the polymer distributes heterogeneously through the material up to a point of saturation and the effects of guest macromolecules on the lattice parameter of PMFs.

Introduction

Control over chemical reactions over many length scales, from individual enzymes to cellular compartments, is a hallmark of biological systems. Nature has found ways to overcome challenges in control over chemical and physical processes through evolution of enzymes, regulation pathways, and cellular organization.[1-3] Virus replication is one such process which involves both viral and host cell components to synthesize more copies of viral structural proteins and genetic material to assemble infectious virions.[4] Because of the complexity of this process, some viruses have evolved to include viral factories in their replication process.[5, 6] Viral factories are organelle-like structures resembling densely packed arrays where components necessary for virus replication are concentrated in a region of the cell, facilitating the assembly of infectious virus particles. The concentration of virus components near the site of assembly enhances the efficiency of the viral replication process and enables their assembly into infectious particles. This chemically determined localization, or partitioning, allows the assembly process to bypass the need to gather components distributed within the cell. The process of viral assembly within these factories provides a bio-inspired approach to self-assembly and catalysis in materials chemistry.

The field of bio-inspired materials looks to nature for inspiration and tools to address complex problems. Among these challenges is the development of catalysts demonstrating selective uptake and activity towards substrates by creating a high local concentration of the substrate available for chemical transformation, much like viral factories drive assembly by accumulating structural components.[7-10] The design and synthesis of materials capable of partitioning select molecules using inspiration from viruses and other protein cages is an ongoing topic of interest. Protein cage materials such as virus-like particles

(VLPs) are a class of materials which self-assemble from multiple copies of a structural protein. Through strategies for encapsulation of a variety of cargos – including proteins, small molecules, and polymers – and modification of their interior, exterior, and the interface between protein subunits, protein cages can be engineered for a variety of applications.[11-18] For example, the use of protein cages as nanoreactors, with encapsulated catalytically active enzymes, has been well studied.[19-22] VLPs are also part of a growing class of *in vivo* enzyme immobilization strategies which avoid problems with enzyme attachment and denaturation seen on other enzyme supports commonly used in industry.[23, 24] Encapsulation of enzymes within VLPs also enforces quaternary structure, protects from degradation by proteases, allows for stoichiometric control of the incorporated catalysts, and allows for generalization of one encapsulation strategy to many enzymes.[25-27]

VLPs derived from bacteriophage P22, for example, assemble from two proteins – a coat protein (CP) which forms the exterior protein shell, and a scaffold protein (SP) which templates CP assembly and is encapsulated during the assembly process.[28] In P22 VLPs, proteins such as catalytically active enzymes are readily incorporated through genetic fusion to the SP, leading to the assembly of VLPs with functional cargo sequestered within the VLP.[29-32] The interior of the cage can be accessed through pores present in the capsid structure. The size of molecules which can enter through these pores can be surprisingly large; the expanded morphology of the P22 capsid allows for transit of molecules up to 2.7 nm in diameter.[33] The design of VLPs with co-encapsulated, sequentially acting enzymes had been suggested to induce a kinetic advantage because the spatial constraint of enzymes in close proximity would purportedly cause the product of one enzyme to directly access the next enzyme without reentering the bulk solution (substrate channeling).[34-37] However, multiple studies of VLPs with co-encapsulated enzymes have shown that proximity alone is insufficient to induce channeling , likely because of the rate of diffusion by enzyme products and the free diffusion of small molecules through the capsid pores.[38]

Protein cages such as VLPs can be assembled into ordered arrays through the addition of oppositely charged macromolecules. The electrostatically driven self-assembly between the protein cage and the linker molecule is screened by ions in solution, allowing for control over the process through modulation of ionic strength.[39, 40] Linker molecules used to assemble arrays from protein cages include polymers, gold nanoparticles, and photoswitchable dyes.[41, 42] P22 VLPs, which carry a high negative charge on their exterior, have been assembled into ordered polymer-templated arrays (PTA) through the addition of cationic G6 polyamidoamine (PAMAM) dendrimers.[43] The arrays are most ordered just below a threshold ionic strength (I_T), where the assembly yields a thermodynamically stable and ordered product. Above I_T, the VLP-dendrimer attraction is too weak to initiate assembly and far below I_T the material is often kinetically trapped in less ordered structures. The assembly of many VLPs into PTAs results in high local concentration of VLPs and VLP components.

The structure of PTAs formed from the expanded morphology of P22 VLPs can be cemented through subsequent treatment with a head-to-head dimer of the decoration protein Dec, which binds to the VLP exterior with extremely high (10-100 nM) affinity and crosslinks the array through a disulfide linkage.[44-46] The templating G6 dendrimer can then be removed by increasing the ionic strength above I_T, leaving behind an ordered crosslinked protein macromolecular framework (PMF) with high negative charge density.[45, 47] PTAs and PMFs assembled from P22 VLPs encapsulating enzymes have been shown to be catalytically active. Because these materials have lower solvation requirements than individual VLPs, they can be concentrated significantly more than individual particles, allowing for acceleration of the reaction rate through use of the same amount of catalyst and substrate in a smaller overall volume.

We have recently described a new strategy for enhancement of catalytic activity in bioinspired materials where substrate partitioning and not co-localization of enzymes is the principle behind the material design.[48] The high local charge of the PMF leads to the partitioning of oppositely charged macromolecule substrates within the framework, resulting in a high local concentration of substrate in proximity to the catalyst. This results in an increase in the turnover rate for the partitioned substrates compared to the reaction catalyzed by enzymes encapsulated within free VLPs. Previous work has also shown that the coating of individual P22 VLPs with a cationic polymer leads to inversion of the VLP charge, but has a minimal effect on the uptake of small molecule substrates.[49] Charged polymers have been used to induce electrostatically-based partitioning due to their high density of ionizable groups.[9, 10] This type of partitioning can directly affect enzymatic activity. For example, the conjugation of organophosphate-binding DNA fragments to phosphotriesterase has been shown to concentrate the substrate near the enzyme increasing the enzyme reaction rate and decreasing the apparent K_M.[50]

In this work, we explore the modification of the PMF to control and alter the charge of the material and ultimately reverse its selective substrate uptake behavior, based on complementary electrostatic interactions, to partition charged molecules. We demonstrate control over the material charge through its titration with a charged polyelectrolyte and show that the material charge directly affects not only the partitioning of charged substrates but also the substrate selectivity of an incorporated enzyme. Instead of modification of the enzyme itself, the PMF acts as a material support which also electrostatically draws substrates out of the bulk solution, increasing the local concentration of the substrate within the material and in the vicinity of the enzyme. Additionally, we have investigated the distribution of the charged polymer within the material, the uptake of macromolecules by the material in different states of charge balance, and the structure of the PMF upon the inclusion of guest macromolecules, representing a step forward in the design of catalytic materials and material supports.

Results and Discussion

To exert control over the charge of P22-based protein macromolecular frameworks and investigate the effects of charge balance within these materials, we drew inspiration from charged polymer brushes. These materials have been shown to localize a large amount of charge in a small volume.[9] We reasoned that through the accumulation of cationic polymers within PMFs we could control and adjust the charge of the framework, allowing control over substrate uptake and catalytic activity **(Figure 1)**.

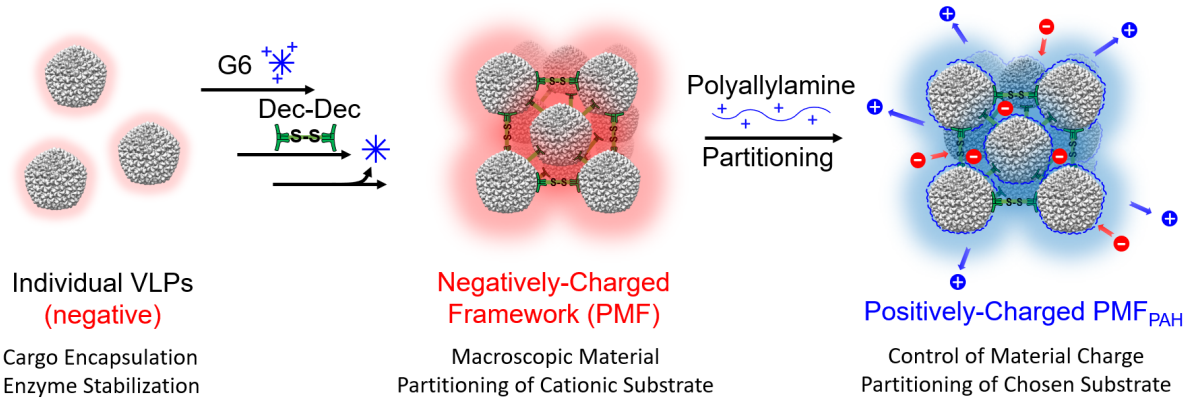

Figure 1. Scheme showing the hierarchical progression from individual VLPs to PMFs bridged by disulfides through the Dec-Dec linker (green) and the expansion of PMFs from a negatively charged material to a material with controllable charge. PMF_{PAH} diagram shows uptake of negatively charged substrates (red spheres) and exclusion of positively charged substrates (blue spheres).

P22 framework materials were prepared from VLPs with an encapsulated enzyme, AdhD ($P22_{E2}$-AdhD), a thermostable (up to 100°C) and pH-stable enzyme.[51] To facilitate the formation of the ordered PMF lattice, we used the E2 variant of the P22 coat protein (CP_{E2}) for the assembly of individual VLPs because the E2 modification on the exterior of the capsid has been shown to produce more ordered materials.[43] P22 VLPs encapsulating the AdhD were expressed, purified, and transformed into the expanded (EX) morphology which can be incorporated into PMFs through previously published methods. SDS-PAGE of the expanded particles showed two bands consistent with the molecular weights of CP_{E2} and AdhD-Scaffolding Protein (AdhD-SP), the two proteins comprising each $P22_{E2}$-AdhD VLP **(Supplementary Figure S1)**. Electron microscopy showed well-formed particles, and the transition to EX was confirmed by size exclusion chromatography-multi angle light scattering (SEC-MALS) and native agarose gel electrophoresis **(Supplementary Figures S2-S5)**. The average molecular weight of the expanded VLPs was 29.4 ± 0.5 MDa, corresponding to 174 ± 8 copies of AdhD-SP encapsulated per particle.

An ordered array of VLPs was initially templated (PTA – polymer templated array) through the introduction of G6 polyamidoamine (PAMAM) dendrimer.[43] Before formation of the PTA, we confirmed that the E2 peptide was intact on CP_{E2} through mass spectrometry **(Supplementary Figure S6)**. The PTA was cemented to form a protein macromolecular framework (PMF) using a ditopic linker composed of head-to-head disulfide bridged dimers of a decoration protein (Dec-Dec) which binds with nanomolar affinity to the exterior of P22 VLPs.[45, 52] The removal of the G6 dendrimer through treatment with high salt buffer yielded the PMF material with high negative charge within its interstitial space as a result of anionic amino acids on the P22 exterior and the linking Dec-Dec protein.

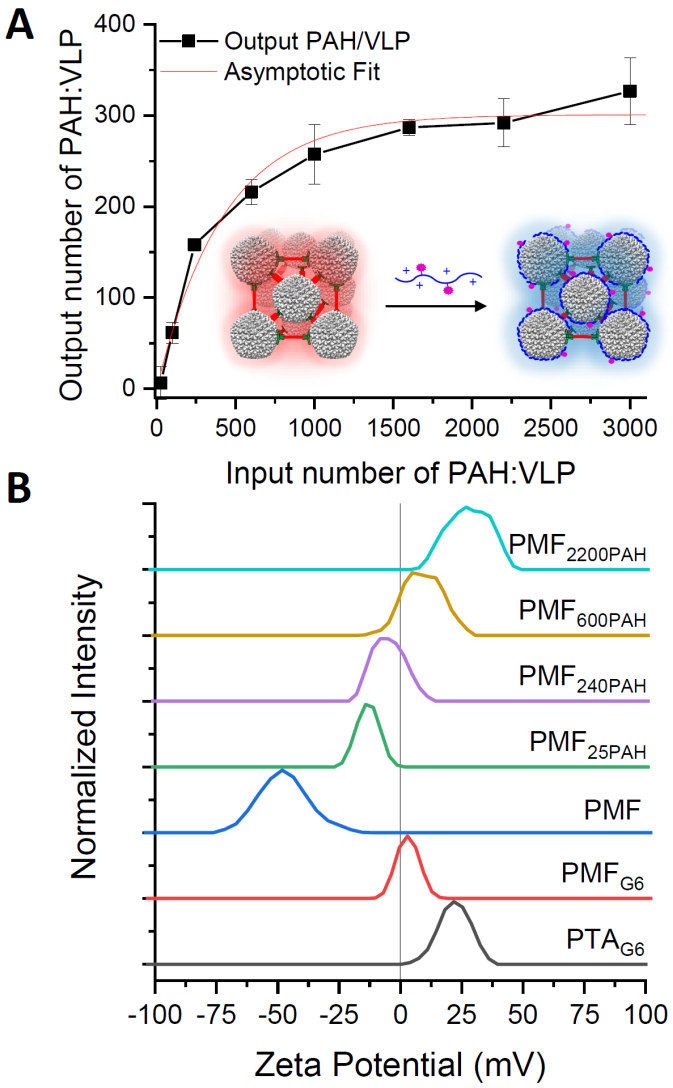

Figure 2. Titration of PMF with PAH. A – Uptake of fluorescently labelled PAH by PMF. The framework becomes saturated at approximately 300 PAH per VLP in the PMF. The red line shows a hyperbolic fit to the data. The VLP concentration was kept constant at 17.0 nM (0.5 mg/mL). The input concentrations of PAH varied from 0.42 µM to 50.9 µM, and the final output saturation concentration at 300 PAH/VLP is 5.11 µM. B – Zeta potential measurements of PMF, precursor materials, and PMF loaded with different amounts of PAH per VLP. PAH-loaded PMF are named by the input PAH/VLP as shown in part A, e.g., $PMF_{2200PAH}$ was prepared with an input of 2200 PAH per VLP. Zeta potential measurements show that the charge of the framework materials can be manipulated through the addition of a small cationic polymer.

To study their uptake of charged macromolecules we titrated assembled PMFs with fluorescently labelled 15 kDa polyallylamine (PAH) **(Figure 2A, Supplementary Figure S7)**. Experiments were performed at low ionic strength (I=46 mM, 20 mM tris and 26 mM NaCl). The interaction between PAH and P22 VLPs is strongest at low ionic strength, allowing for the maximum number of PAH to adsorb and for effects from electrostatic interactions to be most easily detected. At the lower ratios of PAH per VLP investigated (25 to 240 PAH:VLP), the proportion of PAH which partitioned into the framework was approximately 65%,

indicating that the highly negatively charged PMF can readily accommodate the positively charged polymer. As the PAH to VLP ratio was increased, the amount of PAH which localized in the PMF stayed constant at roughly 300 polymer chains per VLP indicating saturation of the framework with PAH. In this work, we will refer to PAH-loaded PMFs as PMF_{xPAH}, where x is the input ratio of PAH per VLP (e.g. PMF_{600PAH} has an input ratio of 600 PAH per VLP of which approximately 215 PAH per VLP are present in the material after its preparation, as shown in **Figure 2A**).

The extent of PAH uptake is likely the result of the charge balance within the material and adsorption of PAH to the negatively charged exterior VLP and Dec-Dec surfaces. As EX P22 VLPs exclude molecules of approximately 4 kDa, the 15 kDa PAH chains are likely concentrated in the interstitial space between VLPs and do not enter the P22 capsid. At high PAH loading, the high localization of cationic polymers on the VLP surface likely inhibits further PAH uptake and results in the observed saturation of the binding sites available on P22 particles within the material. Previous simulations of P22 VLP array formation with G6 dendrimers at similar ionic strengths showed that addition of 1000 G6 dendrimers per VLP resulted in a maximum of about 120 dendrimers per VLP incorporated into the 3D material.[53] This suggests that the overall charge balance within the material's interstitial space imposes a limit for the incorporation of cationic macromolecules into PMFs. Here, the addition of 1000 PAH chains leads to the incorporation of approximately 260 PAH per VLP, indicating that the interaction between P22 VLPs and PAH is stronger than their interaction with the G6 dendrimer. This difference in interaction strength has been shown previously and is possibly the result of higher charge density and more conformational flexibility in PAH.[49, 54]

Zeta potential measurements of the PTA, PMF, and PAH-titrated PMF show the surface charge at each stage of the material synthesis **(Figure 2B, Supplementary Table S1)**. While initial polymer-templated arrays (PTA_{G6}) assembled from P22 VLPs and G6 dendrimers are highly positively charged, these materials are not stable at high ionic strength and are prone to disassembly and structural reorganization.[43] Cementation with the negatively charged Dec-Dec dimer, which binds P22 VLPs at each end, prevents disassembly or reorganization of the material but also changes its charge to neutral overall. The removal of G6 through treatment with a high ionic strength buffer yields a highly negatively charged material.[45] Upon addition of PAH, the charge on the PMF progressively reversed to become quite positive at the point of saturation.

The titration of PAH into the PMF after removal of the templating G6 dendrimer allows for fine control over the PMF material charge **(Figure 2B)**. However, zeta potential measurements do not measure the overall charge within porous materials such as the PMF. In particular, the jump in surface charge from the PMF (-39.5 ± 8.5 mV) to PMF_{25PAH} (-13.2 ± 4.5 mV) is much greater than expected for the addition of a relatively small amount of PAH to the material. We hypothesized that the polymer may stay localized near the framework surface because the addition of a small amount of polymer had a large effect on the material surface charge.

We used super-resolution fluorescence microscopy to qualitatively visualize the distribution of PAH within the PMF. P22 capsids in the assembled framework material were labelled with a fluorescent dye (CF405M, 405 nm) and the framework was subsequently loaded with fluorescently labelled PAH (TRITC, 561 nm). At very low PAH input (25 PAH per P22 VLP; PMF_{25PAH}), the polymer appears to localize at the edges of the PMF and does not penetrate deep into the material, leaving a layer of PAH-coated VLPs around a bulk of unmodified PMF **(Figure 3)**. The partitioning of the polymer to the exterior is consistent with the relatively large shift in zeta potential seen upon the addition of a small amount of PAH to unmodified PAH **(Figure 2B, Figure 4A)**. At intermediate PAH loading (PMF_{240PAH} and PMF_{600PAH}), the polymer penetrates deeper into the framework, but patches are left unmodified, leading to a heterogeneous distribution of PAH in the material. Heterogeneous, disordered products typically form from kinetic processes such as, in this case, the kinetic trapping of PAH in regions within the PMF. These materials likely have areas of high positive charge where PAH has adsorbed to the VLP surface and areas

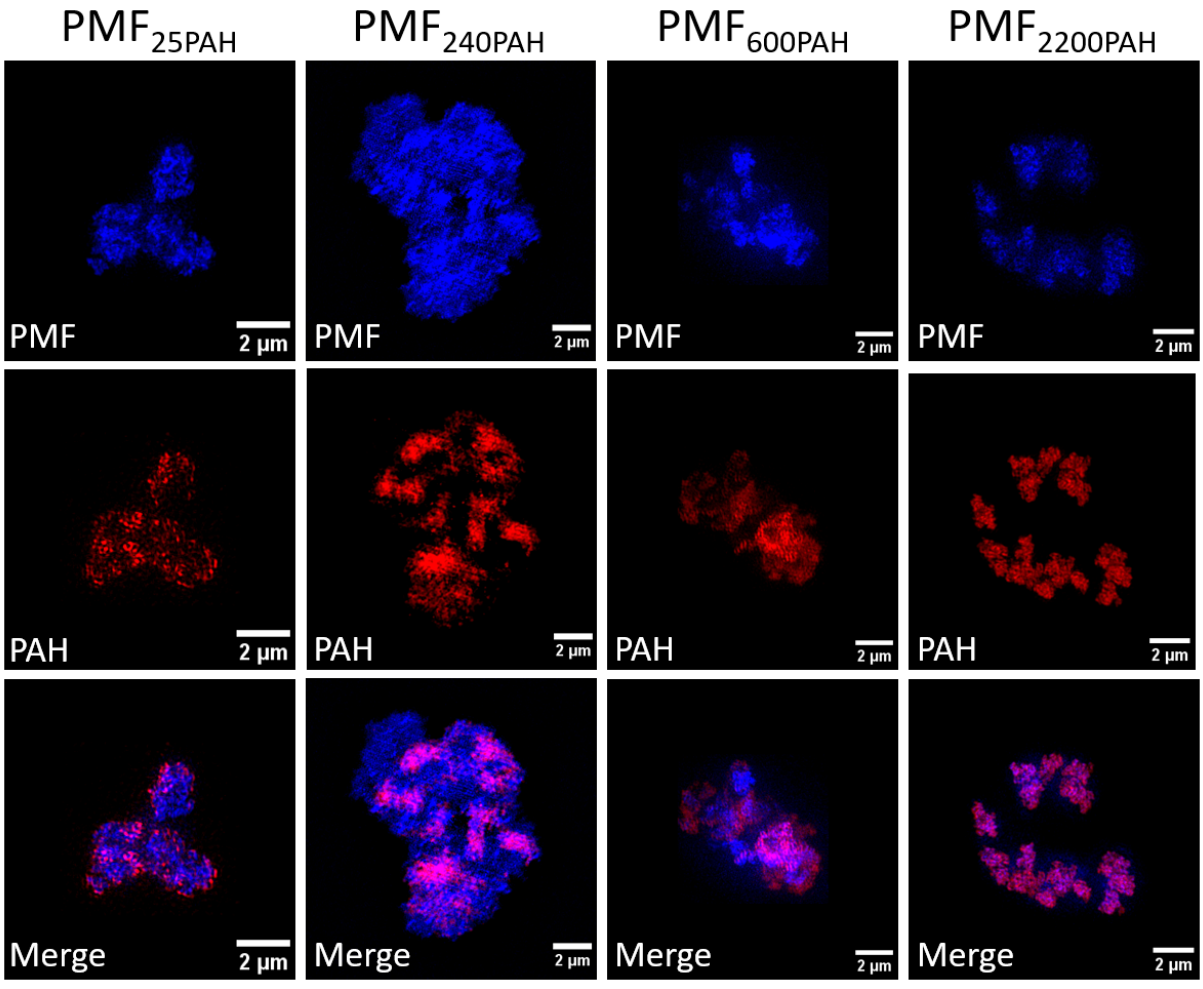

Figure 3. Super-resolution fluorescence microscopy of PMF_{PAH} materials. PMF was fluorescently labelled (blue) and loaded with labelled PAH (red). At low PAH loadings the final product is patchy, containing areas where PAH is present and others where it is not, leading to a material with heterogeneous charge distribution. At high PAH loading, the polymer is evenly distributed through the PMF.

of negative charge where the VLPs remain uncoated, leading to overall relatively neutral zeta potentials but a heterogeneous charge distribution within the material.

At the highest PAH to VLP ratio ($PMF_{2200PAH}$), PAH and PMF colocalize almost entirely, suggesting that the PMF material is saturated by the cationic polymer **(Figure 3)** and homogeneously distributed throughout the PMF. Because VLPs are fully coated with PAH, the zeta potential of the material is highly positive as seen in **Figure 2B**. This result corresponds to saturation of the material with PAH; at this point there are few negatively charged surfaces available.

While fluorescence microscopy provides a qualitative overview of the distribution of PAH in PMFs at different input ratios, these images on their own are not sufficient to give a full understanding of the structural ramifications of the polymer uptake. We analyzed PMF_{PAH} materials by small angle x-ray scattering (SAXS) to quantitatively understand the structural effects of PAH uptake into PMFs **(Figure 4)** and establish the validity of our kinetically trapped uptake model. SAXS data allowed us to confirm the uptake of PAH, the adsorption of the polymer to the P22 exterior, and its distribution in the material.

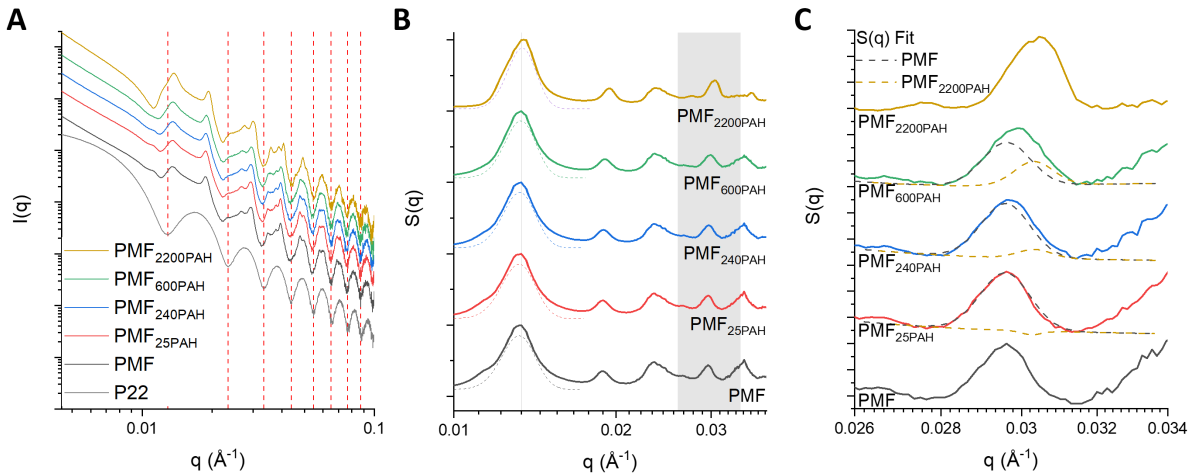

Figure 4. Small angle x-ray scattering of PMF_{PAH} materials. A – SAXS scattering curves for P22 framework materials. Note that the peak minima at high q do not change upon incorporation in the PMF or addition of PAH, indicating that the form factor of P22 does not change. B – Structure factor of PMF materials. Dashed lines are Gaussian fits of the (200) reflection in S(q) around 0.013 Å^{-1}. The overlapped peak of 311 and 420 reflections is highlighted. The shift in the S(q) peak locations is the result of structural changes which occur upon uptake of PAH into the framework. C – Plot of shaded region in B showing the (311/420) reflections of PMF and PMF_{PAH} materials. Dotted lines indicate the deconvoluted contribution of the S(q) of PMF (cyan) and $PMF_{2200PAH}$ (gold) to the S(q) of intermediate materials, showing that these materials consist of interspersed regions of unmodified and PAH-saturated PMF.

PMFs have been established to be ordered and organized into a face-centered cubic (FCC) lattice, confirmed here by indexing peaks arising from the material structure **(Supplementary Figures S8-S12)**. The ordered nature of the material allows for investigation of structural changes in the material through analysis of the structure factor S(q). The presence of S(q) after incorporation of PAH into the framework shows that these PAH bound materials retain their ordered structure. Analysis of the structure factor showed that the uptake of charged macromolecules induced contraction of the interparticle distance in

the PMF **(Figure 4B)**. The lattice parameter of the material upon saturation with PAH decreases from 94.3 nm for PMF to 91.9 nm for $PMF_{2200PAH}$. This shift in the lattice parameter is analogous to that previously seen upon removal of the templating G6 dendrimer from PMFs.[45] The change of the structure factor, however, is not continuous. The lattice constant does not change until 600 PAH/VLP and shows a sudden decrease at 2200 PAH/VLP, indicating that addition of a small amount of polymer does not immediately affect the structure of Dec-Dec and the capsid.

On the other hand, the form factor changes as soon as PAH is added, as seen in the shift of the first I(q) minima toward smaller q, while the minima at high q values are at the same locations as those for the individual P22 VLPs **(Figure 4A)**. This resembles the trend in peak minimum location for scattering curves of core-shell particles in which the shell electron density increases **(Supplementary Figure S13)**.[55] The shift is likely the result of polymer adsorption to the exterior of the VLP, consistent with its uptake into the material as shown in **Figure 2**. Compared to the shift of the minima upon addition of 25 PAH/VLP, the I(q) minima change with increasing PAH uptake between PMF_{25PAH} and PMF_{600PAH} is marginal **(Supplementary Table S2)**. This suggests that the PAH initially compacts on the VLP surface; initial small input could result in full adsorption of the PAH chain to the negatively charged residues of the capsid. When the input reaches 2200 PAH/VLP the form factor minima shift significantly, indicating that the PAH now may not collapse as closely onto the capsid. In addition, the contraction of the lattice constant for $PMF_{2200PAH}$ is possibly the result of the screening of repulsive interactions between VLPs by sufficiently large amounts of PAH and gives further evidence for the uptake of the polymer into the interstitial space within the material. While the particles are ultimately held together by the Dec-Dec linker, this linker can likely undergo a degree of compression or stretching upon changes in electrostatic interactions between VLPs.

To investigate whether the PAH localizes heterogeneously within clusters in the PMF as seen by fluorescence microscopy **(Figure 3)**, rather than distributing homogeneously, we investigated the (311/420) and (531/600) FCC reflections of S(q) as representative examples of the effect of the polymer on the material structure **(Figure 4C, Supplementary Figure S14)**. In this sample series, both (311/420) and (531/600) peaks broadly overlap to appear as single peaks. For the intermediate materials (PMF_{25PAH}, PMF_{240PAH}, and PMF_{600PAH}), these peaks are broader than those of unmodified PMF and $PMF_{2200PAH}$. Their lattice constants are very similar to that of unmodified PMF, and thus the positions of those two peaks are similar as well. However, they show a faint peak tail that cannot be indexed with the same lattice constant of unmodified PMF but can be indexed with the smaller lattice constant of $PMF_{2200PAH}$. Gaussian fitting and deconvolution of the S(q) of the intermediate PAH loading materials shows significant contribution to the S(q) from both unmodified PMF and PAH-saturated PMF, suggesting that regions of both are present in the material. The peak broadening in SAXS analysis of the intermediate PAH-loading materials shows that the proportion of the material showing the PAH-saturated lattice parameter increases as the amount of PAH in the material increases. If the PAH distributed homogeneously in the PMF, we would likely have observed a simple peak shift with no broadening. This data suggests that the presence of PAH in a region of the sample is a binary where the polymer is present or not present, a result of kinetic trapping of the polymer on the surface of the VLPs. The heterogeneity in the material comes from how interspersed and numerous these regions are, not the density of PAH loading across the material. At the highest PAH loading ($PMF_{2200PAH}$), where the framework is saturated, there are very few regions with no PAH adsorbed and the PAH is distributed homogeneously. This quantitatively confirms

the observations about heterogeneous PAH distribution made from the fluorescence microscopy experiment.

We hypothesized that the ability of the framework to host charged macromolecules would be closely related to the overall charge of the PMF material and therefore the degree of PAH loading **(Figure 5A)**. To investigate the uptake of a second charged species into PMF_{PAH}, we titrated supercharged GFP into PMF_{PAH} at different PAH loadings. Titration of supernegative GFP (-GFP) into PMF materials showed higher partitioning of -GFP into PMF with high PAH loading, with the highest uptake observed in $PMF_{2200PAH}$, the highest PAH loading tested **(Figure 5B)**. Interestingly, there is some uptake of -GFP into the unmodified PMF. This is likely the result of the polyelectrolyte nature of the capsid surface, which allows for non-specific interaction with -GFP despite its overall negative charge. The degree of -GFP uptake correlates with the zeta potential of the material before titration, with highly positive materials showing high uptake due to attraction between -GFP and the polymer-modified framework. Similarly, controls measuring the uptake of +GFP showed a decrease in +GFP binding with increasing PAH loading of the material and the more positive zeta potential of the PMF_{PAH} **(Figure 5C)**. Because PAH blocks sites available for interaction by +GFP, there less non-specific uptake of +GFP into $PMF_{2200PAH}$ than there is of -GFP into PMF. Fluorescence microscopy images also show the colocalization of -GFP with PAH and the exclusion of +GFP from regions with PAH **(Supplementary Figure S15)**.

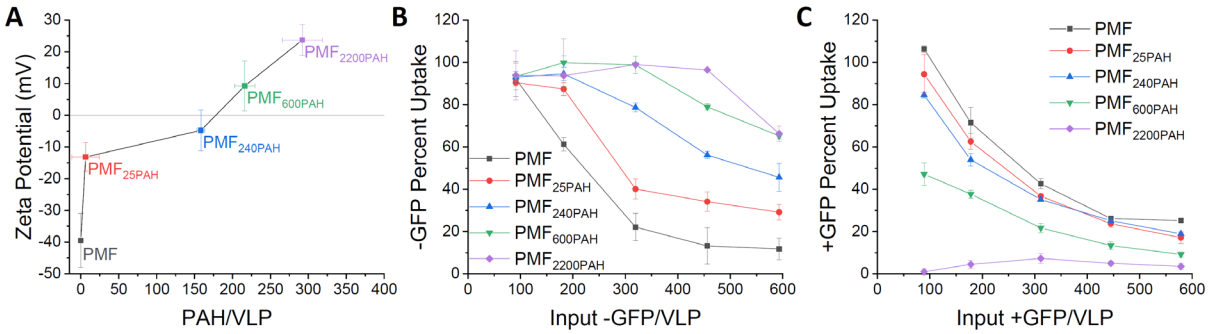

Figure 5. Uptake of -GFP and +GFP into PMF_{PAH} materials. A – Zeta potential of PMF_{PAH} materials as a function of the amount of PAH localized within the framework. B – Percent uptake of -GFP into each PMF_{PAH} material. C – Percent uptake of +GFP into each PMF_{PAH} material. For both uptake experiments, the PMF concentration was kept constant at 1 mg/mL and the input GFP concentration varied from 0.10 mg/mL to 0.65 mg/mL (approximately 90 GFP/VLP to 590 GFP/VLP).

In both experiments, larger input ratios of GFP led to saturation of the framework. Similar to the uptake of PAH, uptake of GFP eventually reaches a point past which a higher input ratio does not lead to incorporation of more GFP. This point occurs much earlier for +GFP into PMF than -GFP into PMF_{PAH}. Most likely this is because the interaction of -GFP with PAH is stronger than the interaction of +GFP with VLPs because of the higher charge density of PAH when compared with P22 VLPs, leading to tighter binding within the material.

The results of the titration study also support our conclusions drawn from the super-resolution microscopy of the framework. As the patches of PAH within the PMF grow, the amount of -GFP taken into the PMF increases steadily, corresponding to the ability of -GFP to adsorb to these regions within the material. The increase in -GFP uptake corresponds to the presence of positively charged regions within PMF_{PAH} which attract -GFP. These are present even in PMF_{25PAH} and PMF_{600PAH}, both which have a negative

overall charge. Hypothetically, PAH could instead distribute homogeneously within the PMF. In this case, the uptake of -GFP would likely stay constant until the material charge reverses to positive upon sufficient addition of PAH, at which point the uptake of +GFP would dramatically increase. Instead, the zeta potential and GFP uptake track closely due to the micro-heterogeneous nature of the material prior to saturation.

To avoid complications arising from the different behaviors of PAH-rich and PAH-poor regions within the same material, we performed all subsequent enzyme activity measurements on two materials – the unmodified PMF, and the fully-loaded $PMF_{2200PAH}$.

Understanding of, and control over, the distribution of polyelectrolyte species in PMFs is a step forward in the design, synthesis, and modification of substrate-selective catalytic materials. Using PMFs prepared with P22 VLPs encapsulating the enzyme AdhD, which uses NADH as a co-factor, we demonstrated altered selectivity and activity toward charged substrates. By conjugation of the NADH to either a negatively or positively charged polyamidoamine (PAMAM) dendrimer (NADH-Den), uptake of the NADH into the PMF is made dependent on the charge of the attached dendrimer **(Supplementary Figures S16-S22)**. In this study, we used negatively ($NADH\text{-}Den^-$) and positively ($NADH\text{-}Den^+$) charged generation 1.5 and generation 2 PAMAM dendrimers, respectively, which previous studies have shown can access both the interstitial space of the PMF and the interior of the VLPs with minimal interference from the capsid or PAH adsorbed to the capsid exterior.[33, 38]

To investigate the selectivity of the materials towards uptake of a charged small molecule substrate, we incubated PMF and $PMF_{2200PAH}$ with varying input NADH-Den to VLP ratios **(Figure 6A)**. At low (109) NADH-Den/VLP, the lowest ratio tested, there is significant uptake of the substrate based on its charge and the charge of the material. Here, the electrostatic forces between the substrate and the material determine its localization. This leads to partitioning of the charged NADH-Den into the framework (for $NADH\text{-}Den^+$ into PMF or $NADH\text{-}Den^-$ into PMF_{PAH}) or exclusion in the case of the framework and dendrimer having the same charge (for $NADH\text{-}Den^-$ into PMF and $NADH\text{-}Den^+$ into PMF_{PAH}). The localization of the NADH-Den in the framework through partitioning creates a high local concentration

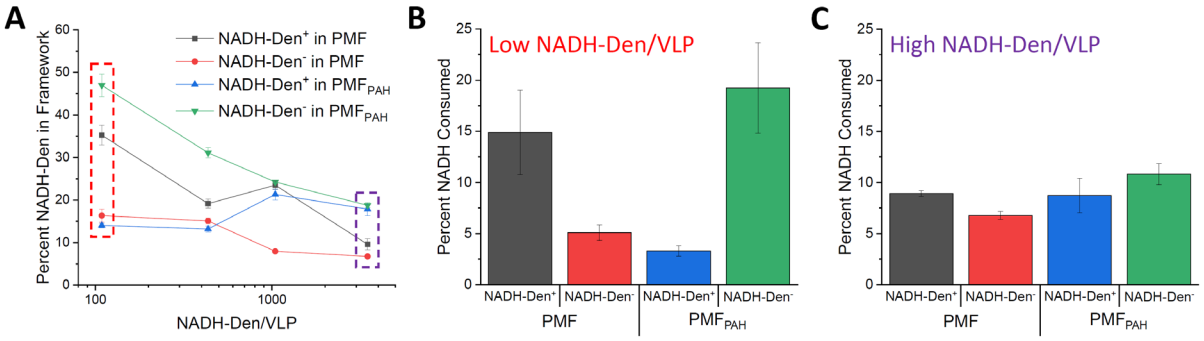

Figure 6. Behavior of framework materials towards charged enzyme substrates. A – NADH-Den percent uptake into the framework as a function of input NADH-Den/VLP ratio. The boxes indicate ratios which were investigated for enzyme activity (red box - 109 NADH-Den/VLP, purple box - 3480 NADH-Den/VLP). B – NADH-Den consumption at an input NADH-Den/VLP ratio where the NADH substrate is partitioned into the material. C – NADH-Den consumption at framework saturation with substrate.

around the VLPs comprising the material, increasing the substrate concentration seen by the encapsulated AdhD.

We performed enzyme activity measurements at two different NADH-Den/VLP ratios with both positively and negatively charged NADH-Den in both unmodified and PAH-saturated PMFs by comparing the consumption of NADH-Den over 20 minutes. Enzyme activity measurements showed that the effect of the framework material charge on the charged substrate partitioning was reflected in the activity of the enzyme encapsulated within the VLPs. When the substrate partitions into the catalytic framework at low (109) NADH-Den/VLP, the consumption of NADH-Den is significantly higher than when it is excluded **(Figure 6B)**, jumping from 3.3% of total substrate consumed to 19.2% (a 5.8-fold increase) for the PMF_{PAH} and from 5.1% to 14.9% (a 2.9-fold increase) for unmodified PMF. This shows that partitioning based on material charge directly affects selectivity and substrate turnover. The higher enzyme activity reflects the increased substrate concentration available to the enzyme, increasing the reaction rate. Similarly, low enzyme activity results from the repulsion of the substrate from the material, lowering the concentration available for enzyme activity. The ability of the partitioned NADH-Den to access encapsulated AdhD shows that while the electrostatic attraction between the framework material and the dendrimer is strong enough to cause partitioning, the interaction is sufficiently reversible that the molecule is mobile within the framework. While there is some residual activity seen for substrates excluded from the material, this is likely due to access by the substrate to VLPs at the edge of the material and from incomplete exclusion from the material. There, the substrate exclusion caused by the colocalization of many VLPs or PAH chains is not as prominent, perhaps allowing diffusion into the VLPs directly from the bulk solution.

We compared the substrate uptake and enzyme activity at 109 NADH-Den/VLP with a higher substrate/VLP ratio to determine the effect of the substrate concentration. As the substrate/VLP ratio increases, the fraction which localizes in the PMF decreases **(Figure 6A)**. At high (3480) NADH-Den/VLP, the highest ratio tested, most of the dendrimer is still found in the bulk solution even when the charge of the dendrimer complements the charge of the framework, likely because the material saturates with the charged NADH-Den. At this NADH-Den:VLP ratio the consumption of NADH-Den by AdhD is approximately equal across each substrate and framework charge **(Figure 6C)**. The high amount of substrate present means that the diffusion of substrate into the material due to a large concentration gradient between the space within the PMF and the bulk solution may overcome the electrostatic forces which lead to substrate concentration or exclusion, regardless of the presence of PAH. As a result, the concentrations locally available to the enzyme are equivalent, resulting in the same activity for each NADH-Den/material pair despite different material charge. As a control, we repeated the experiments with PMF and PMF_{PAH} with an encapsulated enzyme which does not consume NADH (β-glucosidase (CelB), **Supplementary Figure S23)**. This control experiment shows no consumption of NADH-Den, indicating that differences in enzyme activity here are a result of the environment around AdhD produced by the framework.

The increased percent consumption of the $NADH\text{-}Den^-$ at low NADH-Den:VLP by the encapsulated AdhD shows that PAH localized in the PMF allows for uptake of and enzyme activity toward a substrate usually excluded by the PMF material with no PAH bound. The introduction of a cationic polymer component (PAH), which binds to the negatively charged VLP surfaces in the PMF, allows for control over the material charge, the uptake or exclusion of a substrate, and therefore enzyme activity can be directly controlled. Furthermore, the percentage of the substrate consumed is higher for the low NADH-Den:VLP ratio than for the high ratio, indicating that the reaction is more efficient when driven by electrostatic partitioning due to the differential localization and accumulation of the substrate within the material as

compared to the bulk solution. Together, these results show that control over material charge directly allows for control over not only selective uptake but also selective turnover of a charged substrate. One limitation of this system is the relatively low substrate concentration at which the substrate partitions into the PMF. While the percent consumption of the substrate is higher for low NADH-Den/VLP, the overall turnover is higher at high NADH-Den/VLP at the cost of selective activity toward the substrate **(Supplementary Figure S24)**.

Conclusion

Self assembly is a hallmark of biological materials and has long been used as a route to the construction of synthetic materials.[56] Here, we have used self-assembly at different lengthscales to construct functional and tunable materials. Individual virus like particles are directed to self assemble and encapsulate enzyme cargos with high fidelity. These active VLPs are themselves assembled into ordered hierarchical assemblies (PMFs), which carry high negative charge density. The high negative charge inherent in PMFs was used to direct the partitioning of a charged polymer (PAH) into the material to alter and control its overall charge by neutralizing the negatively charged VLP surfaces. The use of partitioning here is not only a part of the synthesis of the material, but also a crucial piece of its function. Through the incorporation of PAH, our material system directs the localization of complementary charged chemical species into the lattice, increasing the local concentration. Thus, the catalytic component of the material, the encapsulated enzyme, is exposed to high local substrate concentration even at low total concentration of substrate, enhancing its catalytic activity. Substrates without charge complementarity to the material are less able to access the enzyme, allowing for control over substrate selectivity. The control over the selectivity of a catalytic system toward a substrate, initiated by simple modification of the material through partitioning of a charged polymer, is a step forward in the development of selective catalytic materials. We have shown that a single-step addition to a material can reverse the localization of a molecule of interest, based on its charge, and that this selectivity reversal is reflected in its catalytic activity towards a charged substrate. At the heart of this biomaterials approach is the tunable catalyst selectivity through modification not of the enzyme but of the material lattice in which is integrated. While modifications of enzyme specificity have reached new heights with the development of methods such as directed evolution, the ability to alter specificity through modification of a customizable enzyme support without modification of the enzyme itself offers a promising alternative.

Experimental

Growth and purification of $P22_{E2}$-AdhD VLPs

E. coli BL21 cells were co-transformed with a pRSF-Duet vector (kanamycin resistance) containing a gene for the E2 variant of P22 coat protein (E2CP) and a pBad vector (ampicillin resistance) containing a gene for P22 scaffold protein fused to alcohol dehydrogenase D. Cells were grown in LB media at 37°C with 50 mg/L ampicillin and 30 mg/L kanamycin until OD_{600} = 0.6 and expression of AdhD-SP was induced with 13.3 mM arabinose. After four hours, expression of E2CP was induced with 0.5 mM IPTG. Cells were grown overnight at room temperature and harvested by centrifugation for 10 minutes at 4500 g. The cell pellet was then resuspended in lysis buffer (50 mM sodium phosphate, 100 mM sodium chloride, pH 7.2) with Pierce Protease Inhibitor and stored at -80°C until later use.

Cell pellets were thawed and incubated with DNAse, RNAse, and lysozyme for 45 minutes at room temperature. The cell suspension was lysed by sonication (Branson Digital Sonifier, 2 minute sonication

time, 50% amplitude, 0.3 s pulse, 0.7 s rest) and then centrifuged at 12000 rpm for 45 minutes at 4°C to remove cellular debris. The lysate was filtered through a 0.45 µm filter and ultracentrifuged at 45000 rpm for 50 minutes through a 35% (w/v) sucrose cushion. The resulting pellet was resuspended in lysis buffer and centrifuged at 17000 rpm to remove lipids. After centrifugation, the supernatant containing the VLPs was run on an S-500 Sephadex column using a BioRad Biologic Duoflow FPLC. Fractions were analyzed for purity by SDS-PAGE, concentrated by ultracentrifugation, and resuspended by rocking with a chosen buffer. Protein concentration was adjusted to approximately 20 mg/mL for storage. Presence of the E2 peptide was confirmed by mass spectrometry on a Waters Synapt G2 HDMS. To prevent cleavage of the E2 peptide, 0.1 mM 4-(2-aminoethyl)benzenesulfonyl fluoride hydrochloride (AEBSF) was added to the resuspended VLPs.

Growth and purification of supercharged GFP variants

E. coli BL21 cells were transformed with a pET29 vector (ampicillin resistance) containing a gene for supernegative GFP (-GFP) or superpositive GFP (+GFP). Vectors were obtained from Addgene (Plasmid #62936 and #62937). Cells were grown in LB media at 30°C with 50 mg/L ampicillin until OD_{600} = 0.6 and expression of GFP was induced with 0.5 mM IPTG. Cultures were grown overnight at 30°C and harvested by centrifugation for 10 minutes at 4500 g. Cell pellets were stored at -80°C until later use.

For -GFP, cell pellet was resuspended in 50 mM sodium phosphate, 100 mM sodium chloride, pH 7.8 buffer. The resuspended pellet was incubated with DNAse, RNAse, and lysozyme for 45 minutes at room temperature. The cell suspension was lysed by sonication (Branson Digital Sonifier, 2 minute sonication time, 50% amplitude, 0.3 s pulse, 0.7 s rest) and then centrifuged at 12000 rpm for 45 minutes at 4°C to remove cellular debris. The lysate was then filtered through a 0.45 µm filter. The solution was then run on a Roche cOmplete His-Tag purification column using a Biorad Duoflow FPLC. The protein was eluted using a 10-500 mM imidazole gradient. Fractions were analyzed for purity by SDS-PAGE and pooled. Imidazole was removed by dialysis against the desired buffer. GFP was concentrated and buffer-exchanged using Amicon centrifugal filters. The procedure for purification of +GFP was the same, but 2 M NaCl was added to all buffers before FPLC to allow for binding of +GFP to the column.

Growth purification, and oxidation of DecS134C

E. coli BL21 cells were transformed with a pET Duet vector (ampicillin resistance) containing a gene encoding for DecS134C. Cells were grown in LB media at 37°C with 50 mg/L ampicillin until OD_{600} = 0.6 and expression of DecS134C was induced with 1 mM IPTG. Cells were grown overnight and harvested by centrifugation for 10 minutes at 4500 g. Cell pellets were stored at -80°C until later use.

Cell pellets were resuspended in lysis buffer and incubated with DNAse, RNAse, and lysozyme for 45 minutes at room temperature. The cell suspension was lysed by sonication (Branson Digital Sonifier, 2 minute sonication time, 50% amplitude, 0.3 s pulse, 0.7 s rest) and then centrifuged at 12000 rpm for 45 minutes at 4°C to remove cellular debris. The lysate was filtered through a 0.45 µm filter. The solution was then run on a Roche cOmplete His-Tag purification column using a Biorad Duoflow FPLC. The protein was eluted using a 10-500 mM imidazole gradient. Fractions were analyzed for purity by SDS-PAGE and UV-Vis spectroscopy. Fractions with an A_{280}:A_{260} above 1 were pooled and dialyzed to remove imidazole.

Because DecS134C is susceptible to modification at the terminal cysteine, the protein was reduced and reoxidized to form head to head Dec-Dec dimers. DecS134C was incubated for 4 hours at 4°C with 5 mM

dithiothreitol (DTT) and then dialyzed overnight to remove DTT and small molecules. DecS134C was then oxidized through incubation with 20 µM copper (II) sulfate at 4°C overnight. The solution was dialyzed overnight again to remove copper (II) and centrifuged to remove precipitates which formed during the oxidation.

Expansion of $P22_{E2}$-AdhD

4 mL of sodium dodecyl sulfate (SDS, initial 0.1% wt) in lysis buffer was added to 4 mL $P22_{E2}$-AdhD solution (initial 1 mg/mL) in lysis buffer. The solution was mixed constantly for 5 minutes, after which 17 mL lysis buffer was added. The solution was then ultracentrifuged at 45000 rpm for 50 minutes three times with fresh changes of lysis buffer. Expansion was confirmed through SEC-MALS.

Size Exclusion Chromatography-Multi Angle Light Scattering (SEC-MALS)

Samples were separated on a Wyatt Technologies WTC-200S 5 µM, 2000 Å, 7.8 x 300 mm size exclusion column using an Agilent 1200 HPLC with a flow rate of 0.7 mL/minute in a 50 mM sodium phosphate, 100 mM sodium chloride, 200 ppm sodium azide, pH 7.2 buffer. Samples were detected using an Agilent UV-Vis detector, a Wyatt HELEOS multi-angle light scattering (MALS) detector, and an Optilab rEX differential refractometer. The number average molecular weight (M_n) of VLPs was calculated Astra 5.3.14 software (Wyatt Technology Corporation) based on the molecular weight distribution. Equation 1 was used the calculate the molecular weight:

$$M = \frac{R\,(\theta)}{\frac{4\pi^2 n_0^2}{N_A \lambda_0^4}\left(\frac{dn}{dc}\right)^2 c\,P(\theta)} \quad \text{(Eq. 1)}$$

$R\,(\theta)$ - Excess Rayleigh ratio from solute
n_0- Solvent refractive index
N_A - Avogadro's number
λ_0 - Vacuum wavelength of incident light
$\left(\frac{dn}{dc}\right)$ – Specific refractive index increment in mL/g (for proteins: 0.1850)
M - Molar mass in g/mol
c - Solute concentration (w/v)
$P(\theta)$ - Form factor relating to angular variation and mean square radius

Sodium dodecyl sulfate – polyacrylamide gel electrophoresis (SDS-PAGE)

Polyacrylamide resolving gels were cast from 5 mL of 1.5 M tris pH 8.8, 4.5 mL of 40% acrylamide (19:1 acrylamide:bisacrylamide), 5.33 mL of water, 75 µL of 20% SDS in water, 75 µL of 10% ammonium persulfate (APS) in water, 25 µL tetramethylethylenediamine (TEMED) immediately after mixing. The solution was leveled with n-butanol. After 30 minutes, butanol was removed and the stacking gel was cast from 620 µL of 0.5 M tris pH 6.8, 625 µL of 40% acrylamide (19:1 acrylamide:bisacrylamide), 3.7 mL of water, 25 µL of SDS in water, 50 µL of 10% APS in water, and 5 µL TEMED.

Samples for SDS-PAGE were prepared by adding 20 µL of sample to 10 µL of SDS loading dye. Samples were heated at 100°C for 12 minutes before loading onto a 12% acrylamide gel. Gels were run at a constant current of 36 A for 50 minutes. The ladder used was PageRuler Prestained Protein Ladder, 10 to

180 kDa (ThemoFisher). Gel was stained with Coomassie Blue, destained, and imaged using an Enduro GDS II.

Native Agarose Gel Electrophoresis

A 0.8% wt agarose gel was prepared in 50 mL of tris-EDTA (40 mM tris, 5 mM acetate, and 1 mM ethylenediaminetetraacetic acid (EDTA)). 5 µL of non-denaturing loading buffer was added to a 20 µL protein sample at 1 mg/mL followed by loading 20 µL onto the polymerized gel. Samples were run on the agarose gel for 1 hour at 100 V in tris-EDTA buffer. The gel was stained with Coomassie Blue, destained, and imaged using an Enduro GDS II.

Synthesis of PAH-FITC and PAH-TRITC

80 mg of 15 kDa poly(allylamine HCl) (0.85 mmol allylamine monomers) was dissolved in 8 mL sodium tetraborate buffer (50 mM, pH 8.7). To this was added 0.011 mmol fluorescein isothiocyanate (FITC, ε_{494} = 70000 M-1cm-1) or tetramethylrhodamine (TRITC, ε_{550} = 100000 $M^{-1}cm^{-1}$) dissolved in 0.5 mL dimethyl sulfoxide (DMSO). The input ratio of dye molecules to polymer chains was 2:1. The reaction was incubated overnight at room temperature. After incubation, the solution was transferred to 500-1000 Da molecular weight cut off (MWCO) dialysis tubing. The solution was dialyzed overnight first against water to allow for removal of sodium tetraborate buffer and unreacted FITC or TRITC. The solution was then dialyzed overnight against 2 M sodium chloride to ensure condensation of chloride counterions, followed by dialysis against water again. The PAH-FITC or PAH-TRITC was lyophilized to a powder.

Determination of Concentrations by UV-Vis Spectroscopy

Protein concentrations were determined through absorbance measurements on an Agilent Cary 8454 UV-Vis Diode Array System. Protein concentrations were measured using extinction coefficients at 280 nm calculated using the Expasy ProtParam tool after 1:10 dilution in 6 M guanidine HCl to denature proteins. For samples containing G6 or PAH, samples were first diluted 1:2 with 4 M NaCl to remove contribution to absorbance readings from scattering. Concentrations of NADH and NADH-dendrimer conjugates were measured using ε_{340}= 6.22 $mM^{-1}cm^{-1}$. Data was exported using Spectragryph.[57]

PMF Assembly

To form a polymer templated array (PTA) of P22 VLPs, G6 PAMAM dendrimers in lysis buffer were added to a solution of expanded $P22_{E2}$-AdhD VLPs in lysis buffer for a final VLP concentration of 1 mg/mL during assembly and G6:VLP ratio of 1000:1. The solution was incubated for 2 hours at room temperature followed by refrigeration overnight.

To cement the PTA into a protein macromolecular framework (PMF_{G6}), a solution of Dec-Dec in lysis buffer was added to the PTA. To ensure high occupancy of Dec binding sites on P22 VLPs, Dec-Dec was added in an 80:1 ratio of head-to-head dimers to VLPs. The material was incubated for 2 hours at room temperature followed by refrigeration overnight. After cementation with Dec-Dec, the material was centrifuged at 5000 rpm, supernatant removed, and pellet resuspended in an equal volume of 20 mM tris, 26 mM NaCl, pH 7.2 (I=46 mM tris buffer). The centrifugation and resuspension process was repeated three times to remove unbound Dec and residual phosphate buffer.

G6 was removed from the framework by raising the ionic strength to yield a highly negatively charged framework (PMF). PMF_{G6} was centrifuged at 5000 rpm for 2 minutes and the supernatant was removed. The resulting pellet was resuspended in the same amount of 20 mM tris, 400 mM NaCl (I=516 mM tris buffer) and incubated for five minutes. The material was washed twice more to fully remove G6. The final material (PMF) was again washed with I=46 mM tris buffer. Concentration of the framework was determined by the above method. The PMF was stored at a concentration of 1.5 mg/mL VLP concentration.

Zeta potential measurements

Zeta potential measurements were taken on a Malvern Instruments Zetasizer Nano ZS. Sample concentration was approximately 0.1 mg/mL and measurements were done in 10 mM tris, 13 mM NaCl. The Smoluchowski approximation was used to convert the electrophoretic mobility to zeta potential.

PMF Uptake of Supercharged GFP

Supercharged GFP (+36 GFP or -30 GFP) in I=46 mM tris buffer was added to PMF in the same buffer for a final VLP concentration of 1 mg/mL and a final GFP concentration between 0.10 mg/mL (approximately 90 GFP/VLP) and 0.65 mg/mL (approximately 590 GFP/VLP). Samples were incubated at room temperature overnight followed by centrifugation at 10000 xg. To determine the amount of GFP remaining in the supernatant, the absorbance of the supernatant was measured on an Agilent Cary 8454 UV-Vis Diode Array System. The absorbance spectrum of supercharged GFP at each input ratio was measured as a control.

PMF Uptake of PAH-FITC

PAH-FITC in I=46 mM tris buffer was added to PMF in the same buffer. The concentration of VLPs in the samples was kept constant at 0.5 mg/mL while the input concentration of PAH-FITC was varied from 25:1 PAH:VLP to 3000:1 (0.42 μM to 50.9 μM). Samples were incubated at room temperature overnight followed by centrifugation at 10000 xg. To determine the amount of PAH-FITC remaining in the supernatant, the absorbance of the supernatant was measured on an Agilent Cary 8454 UV-Vis Diode Array System. The absorbance spectrum of PAH-FITC at each input ratio was measured as a control.

PMF_{PAH} Assembly

PAH-TRITC in I=46 mM tris buffer was added to PMF in the same buffer. The VLP concentration during assembly was 1 mg/mL, and the PAH/VLP ratio was varied from 25:1 to 2200:1. The material was incubated for 2 hours at room temperature followed by refrigeration overnight. To remove unbound PAH, the sample was centrifuged at 3000 rpm for 3 minutes and the supernatant replaced with fresh buffer twice. Concentration of the framework was determined by the above method. PMF_{PAH} was stored at 1.5 mg/mL VLP concentration.

GFP Uptake Experiment

PMF or PMF_{PAH} at 1 mg/mL VLP concentration was incubated overnight with -GFP or +GFP (ranging from 0.05 mg/mL to 0.65 mg/mL) in I=46 mM tris buffer. After incubation, samples were centrifuged at 3000 rpm for 3 minutes to pellet PMF. To determine the amount of GFP taken into the PMF, 2 μL aliquots of supernatant were analyzed on a Take3 plate using a BioTek Cytation 5 Cell ImagingMulti-Mode Reader. Samples were done in triplicate.

Sample Preparation for Super-Resolution Microscopy

Pre-assembled PMF was labelled with CF405M-maleimide (Biotium) through incubation overnight. The material was centrifuged at 3000 rpm for 3 min and washed 3 times to remove unreacted dye. The CF405-labelled PMF was used to prepare PMF_{PAH} at different PAH loading as described above. For samples with +GFP or -GPF, GFP was added to a final ratio of 100 GFP/VLP and incubated overnight. Samples in I=46 mM tris buffer were loaded onto a glass slide with a coverslip and immediately imaged to minimize evaporation of solvent.

Super-Resolution Microscopy

Images of fluorescently-labelled PMF_{PAH} were collected on a DeltaVision OMX SR Super-Resolution Microscope. Fluorophore excitation was achieved using 405 nm (CF405, PMF), 488 nm (GFP), and 561 nm (TRITC, PAH) laser lines. Images were captured using maximum 25 ms exposure times. The step size was fixed at 0.125 µm with sample thickness varying between 3 µm and 10.5 µm. Reconstruction and chromatic alignment was performed in SoftWoRx.

Small Angle X-Ray Scattering (SAXS) Measurements

SAXS measurements were performed at beamline 12 ID-B at the Advanced Photon Source, Argonne National Lab. Measurements were conducted at 14 keV and scattering data was collected using a Pilatus 2M detector. The scattering angle was calibrated using silver behenate as a standard. One-dimensional scattering profiles were obtained by averaging two-dimensional scattering patterns. The data were represented as scattering intensity as a function of scattering vector q:

$$q = \frac{4\pi}{\lambda} sin\theta$$

Where θ is half of the scattering angle 2θ and λ is the x-ray wavelength used for measurements.

SAXS sample preparation

All samples for SAXS were adjusted to a VLP concentration of 0.8 mg/mL. Background subtraction was done by subtracting the scattering profile from the sample buffer from the scattering profile of the sample.

Synthesis of NADH-Dendrimer

NADH-Dendrimer conjugates were synthesized through procedures similar to those previously published.[48] Some volumes and separation steps have been changed. NMR and UV-Vis characterization data are available in **Figures S14-S20**.

NAD^+-Br

1 g (1.51 mmol) of NAD^+ was dissolved in 15 mL 500 mM sodium acetate buffer, pH 4.5. The solution was stirred rapidly as 0.4 mL (4.52 mmol, 3 eq) of Br_2 were added dropwise through a septum. Progress of the reaction was tracked by monitoring the shift of the NAD^+ UV-Vis λ_{max} from 259 nm to 265 nm. After 2 hours, the solution was washed with chloroform to remove excess unreacted bromine until the organic layer was clear. The aqueous layer was recovered and filtered through a 200 Da MWCO nanofiltration membrane under 50 psi to remove residual bromine and sodium acetate. The product was lyophilized and stored at -20°C until needed.

NADH-Br

16 mL of freshly prepared 1.3% (w/v) sodium bicarbonate buffer was bubbled with nitrogen for 30 minutes. After bubbling, 0.24 g (0.32 mmol) of NAD^+-Br and 0.12 g (0.65 mmol, 2 eq) of sodium dithionite were added to the bicarbonate buffer. The solution turned a bright yellow color upon addition of dithionite. The reaction was kept blanketed under nitrogen and covered to protect from light. Progress of the reaction was tracked by monitoring the A_{265}:A_{340} ratio as it approached 3.

After 2 hours, the solution was transferred to centrifuge tubes and immediately precipitated through addition of 10 x volume of -20°C acetone. The tubes were centrifuged at 4500 xg for 5 minutes, and the supernatant was discarded. The pellet was resuspended in water, lyophilized, and stored at -20°C until needed.

NADH-Linker

0.3 g NADH-Br was dissolved in 8 mL DMSO, blanketed with nitrogen, and heated to 60°C. 0.248 mL (1.7 mmol) of 2,2'-(ethylenedioxy)bis(ethylamine) linker was added to 8 mL DMSO and added to the NADH-Br solution. The reaction was kept at 60°C under nitrogen, covered to protect from light, and allowed to react overnight.

The reaction solution was transferred to centrifuge tubes and centrifuged to remove residual undissolved salts. The supernatant was then immediately precipitated though addition of 10 x volume of -20°C acetone followed by centrifugation at 4500 xg for 5 minutes. The supernatant was discarded and the pellet was dissolved in water followed by a second precipitation with -20°C acetone. The supernatant was discarded, the pellet was dissolved in water, and finally filtered through a 200 Da MWCO ultrafiltration membrane under 50 psi to remove unreacted linker and residual DMSO. The product was lyophilized and stored at -20°C until needed.

NADH-Den$^-$

Freshly prepared 2% (w/v) sodium bicarbonate buffer and bubbled with nitrogen for 1 hr. In a separate flask, 0.06 mmol generation 1.5 PAMAM dendrimer (G1.5) was added to 3 mL of 100 mM MES buffer, pH 4.7. The pH was adjusted to between 4.7 and 5. After pH adjustment, 285 mg EDC was added to the solution, which was then bubbled with nitrogen for 1 hr.

40 mg (0.012 mmol, 2 per dendrimer) NADH-Linker was dissolved in 3 mL of the sodium bicarbonate buffer and added through a septum to the G1.5/EDC solution. The reaction was blanketed with nitrogen, covered to protect from light, and allowed to react overnight. The solution was then dialyzed against water using 2 kDa MWCO membranes overnight at 4°C to remove unreacted NADH-linker, lyophilized, and stored at -20°C until needed.

NADH-Den$^+$

0.1 g NADH-Br was dissolved in 2.9 mL DMSO, blanketed with nitrogen, and heated to 60°C. 0.022 mmol generation 2 PAMAM Dendrimer (G2) was added to 2.9 mL of DMSO and added to the NADH-Br solution. The reaction was kept at 60°C under nitrogen, covered to protect from light, and allowed to react overnight.

The reaction solution was transferred to centrifuge tubes and centrifuged to remove residual undissolved salts. The supernatant was then immediately precipitated though addition of 10 x volume of -20°C acetone followed by centrifugation at 4500 xg for 5 minutes. The pellet was resuspended in water and dialyzed against a 2 kDa MWCO membrane overnight to remove unreacted NADH-Br.

Nuclear Magnetic Resonance (NMR) Measurements

Approximately 10 mg of sample was dissolved in 0.5 mL D_2O. Measurements were made using a Varian 400 MHz Inova NMR spectrometer.

Enzyme Activity Assays

To determine catalytic activity of each VLP-based catalytic material, the framework was incubated with NADH-Den for 10 minutes followed by addition of acetoin (final concentration 50 mM). After 19 minutes, a high salt buffer (final NaCl concentration 500 mM) was added to break the electrostatic interactions between the material and the NADH-Den, and the sample was centrifuged for 1 minute at 10000 xg. The A_{340} of the supernatant was measured on a Take3 plate using a BioTek Cytation 5 Cell ImagingMulti-Mode Reader. To ensure that there was no interference from scattering by the framework, the absorbance was compared to a sample with no acetoin addition to determine percent consumption of the NADH-Den. As a control, the experiment was repeated with PMF and PMF_{PAH} made with P22 VLPs with encapsulated β-glucosidase, which does not consume NADH. All samples were done in triplicate.

Associated Content

Supporting Information. Characterization of VLPs by SDS-PAGE, TEM, native agarose gel electrophoresis, and MS. Zeta Potential of PAH. Indexed SAXS I(q) and S(q) plots, modeling of SAXS data to capsid shell density, analysis of S(q) (531/600) reflection. NMR and UV-Vis spectra of NADH-Den and precursors. Enzyme activity experimental control and turnover numbers. PMF_{PAH} material zeta potentials and lattice parameters.

Acknowledgements

This work was supported in part by grants from the National Science Foundation (CMMI-1922883 and EEC-1720625) and the Human Frontier Science Program (HFSPO RGP0012/2018). The authors thank the Indiana University Electron Microscopy Center, the Indiana University Nuclear Magnetic Resonance (NMR) Facility, the Indiana University Nanoscale Characterization Facility, and the Light Microscopy Imaging Center (LMIC; Indiana University) for access to their instrumentation. The OMX-SR microscope at the LMIC was acquired under the National Institutes of Health (NIH) award NIH1S10OD024988-01. This research used resources of the Advanced Photon Source, a U.S. Department of Energy (DOE) Office of Science User Facility, operated for the DOE Office of Science by Argonne National Laboratory under Contract No. DE-AC02-06CH11357. SAXS data were collected at Beamline 12-ID-B, Advanced Photon Source, Argonne National Laboratory.

References

1. Bar-Even, A.; Noor, E.; Savir, Y.; Liebermeister, W.; Davidi, D.; Tawfik, D. S.; Milo, R., The Moderately Efficient Enzyme: Evolutionary and Physicochemical Trends Shaping Enzyme Parameters. *Biochemistry* **2011,** *50* (21), 4402-4410.
2. Atkinson, D. E., REGULATION OF ENZYME FUNCTION. *Annu. Rev. Microbiol.* **1969,** *23* (1), 47-68.
3. Giessen, T. W.; Silver, P. A., Encapsulation as a Strategy for the Design of Biological Compartmentalization. *J. Mol. Biol.* **2016,** *428* (5, Part B), 916-927.
4. Louten, J., Chapter 4 - Virus Replication. In *Essential Human Virology*, Louten, J., Ed. Academic Press: Boston, 2016; pp 49-70.
5. Netherton, C.; Moffat, K.; Brooks, E.; Wileman, T., A Guide to Viral Inclusions, Membrane Rearrangements, Factories, and Viroplasm Produced During Virus Replication. Elsevier: 2007; pp 101-182.
6. Novoa, R. R.; Calderita, G.; Arranz, R.; Fontana, J.; Granzow, H.; Risco, C., Virus factories: associations of cell organelles for viral replication and morphogenesis. *Biol. Cell* **2005,** *97* (2), 147-172.
7. Mitchell, S.; Qin, R.; Zheng, N.; Pérez-Ramírez, J., Nanoscale engineering of catalytic materials for sustainable technologies. *Nat. Nanotechnol.* **2021,** *16* (2), 129-139.
8. Rae, B. D.; Long, B. M.; Badger, M. R.; Price, G. D., Functions, Compositions, and Evolution of the Two Types of Carboxysomes: Polyhedral Microcompartments That Facilitate CO2 Fixation in Cyanobacteria and Some Proteobacteria. *Microbiol. Mol. Biol. Rev.* **2013,** *77* (3), 357-379.
9. Kusumo, A.; Bombalski, L.; Lin, Q.; Matyjaszewski, K.; Schneider, J. W.; Tilton, R. D., High Capacity, Charge-Selective Protein Uptake by Polyelectrolyte Brushes. *Langmuir* **2007,** *23* (8), 4448-4454.
10. Liu, Q.; Yu, B.; Ye, W.; Zhou, F., Highly Selective Uptake and Release of Charged Molecules by pH-Responsive Polydopamine Microcapsules. *Macromol. Biosci.* **2011,** *11* (9), 1227-1234.
11. Douglas, T.; Young, M., Viruses: Making friends with old foes. *Science* **2006,** *312* (5775), 873-875.
12. Patterson, D. P.; Rynda-Apple, A.; Harmsen, A. L.; Harmsen, A. G.; Douglas, T., Biomimetic Antigenic Nanoparticles Elicit Controlled Protective Immune Response to Influenza. *Acs Nano* **2013,** *7* (4), 3036-3044.
13. Tetter, S.; Hilvert, D., Enzyme Encapsulation by a Ferritin Cage. *Angew. Chem., Int. Ed.* **2017,** *56* (47), 14933-14936.
14. Chen, C.; Daniel, M.-C.; Quinkert, Z. T.; De, M.; Stein, B.; Bowman, V. D.; Chipman, P. R.; Rotello, V. M.; Kao, C. C.; Dragnea, B., Nanoparticle-Templated Assembly of Viral Protein Cages. *Nano Lett.* **2006,** *6* (4), 611-615.
15. Comellas-Aragones, M.; Engelkamp, H.; Claessen, V. I.; Sommerdijk, N.; Rowan, A. E.; Christianen, P. C. M.; Maan, J. C.; Verduin, B. J. M.; Cornelissen, J.; Nolte, R. J. M., A virus-based single-enzyme nanoreactor. *Nat. Nanotechnol.* **2007,** *2* (10), 635-639.
16. Edwardson, T. G. W.; Levasseur, M. D.; Tetter, S.; Steinauer, A.; Hori, M.; Hilvert, D., Protein Cages: From Fundamentals to Advanced Applications. *Chem. Rev.* **2022,** *122* (9), 9145-9197.
17. McNeale, D.; Dashti, N.; Cheah, L. C.; Sainsbury, F., Protein cargo encapsulation by virus-like particles: Strategies and applications. *WIREs Nanomedicine and Nanobiotechnology* **2023,** *15* (3), e1869.
18. Glasgow, J.; Tullman-Ercek, D., Production and applications of engineered viral capsids. *Appl. Microbiol. Biotechnol.* **2014,** *98* (13), 5847-5858.
19. O'Neil, A.; Prevelige, P. E.; Douglas, T., Stabilizing viral nano-reactors for nerve-agent degradation. *Biomaterials Science* **2013,** *1* (8), 881-886.
20. Maity, B.; Fujita, K.; Ueno, T., Use of the confined spaces of apo-ferritin and virus capsids as nanoreactors for catalytic reactions. *Curr. Opin. Chem. Biol.* **2015,** *25*, 88-97.

21. Aumiller, W. M., Jr.; Uchida, M.; Douglas, T., Protein cage assembly across multiple length scales. *Chem. Soc. Rev.* **2018,** *47* (10), 3433-3469.
22. Fiedler, J. D.; Brown, S. D.; Lau, J. L.; Finn, M. G., RNA-Directed Packaging of Enzymes within Virus-like Particles. *Angewandte Chemie-International Edition* **2010,** *49* (50), 9648-9651.
23. Ölçücü, G.; Klaus, O.; Jaeger, K.-E.; Drepper, T.; Krauss, U., Emerging Solutions for in Vivo Biocatalyst Immobilization: Tailor-Made Catalysts for Industrial Biocatalysis. *ACS Sustainable Chemistry & Engineering* **2021,** *9* (27), 8919-8945.
24. Seo, M.-J.; Schmidt-Dannert, C., Organizing Multi-Enzyme Systems into Programmable Materials for Biocatalysis. *Catalysts* **2021,** *11* (4), 409.
25. Jordan, P. C.; Patterson, D. P.; Saboda, K. N.; Edwards, E. J.; Miettinen, H. M.; Basu, G.; Thielges, M. C.; Douglas, T., Self-assembling biomolecular catalysts for hydrogen production. *Nat. Chem.* **2016,** *8* (2), 179-185.
26. Sharma, J.; Uchida, M.; Miettinen, H. M.; Douglas, T., Modular interior loading and exterior decoration of a virus-like particle. *Nanoscale* **2017,** *9* (29), 10420-10430.
27. Sharma, J.; Douglas, T., Tuning the catalytic properties of P22 nanoreactors through compositional control. *Nanoscale* **2020,** *12* (1), 336-346.
28. Prevelige, P. E.; Thomas, D.; King, J., Scaffolding protein regulates the polymerization of P22 coat subunits into icosahedral shells in vitro. *J. Mol. Biol.* **1988,** *202* (4), 743-757.
29. O'Neil, A.; Reichhardt, C.; Johnson, B.; Prevelige, P. E.; Douglas, T., Genetically Programmed In Vivo Packaging of Protein Cargo and Its Controlled Release from Bacteriophage P22. *Angewandte Chemie-International Edition* **2011,** *50* (32), 7425-7428.
30. Patterson, D. P.; Prevelige, P. E.; Douglas, T., Nanoreactors by Programmed Enzyme Encapsulation Inside the Capsid of the Bacteriophage P22. *ACS Nano* **2012,** *6* (6), 5000-5009.
31. McCoy, K.; Selivanovitch, E.; Luque, D.; Lee, B.; Edwards, E.; Caston, J. R.; Douglas, T., Cargo Retention inside P22 Virus-Like Particles. *Biomacromolecules* **2018,** *19* (9), 3738-3746.
32. Essus, V. A.; Souza Júnior, G. S. E.; Nunes, G. H. P.; Oliveira, J. D. S.; De Faria, B. M.; Romão, L. F.; Cortines, J. R., Bacteriophage P22 Capsid as a Pluripotent Nanotechnology Tool. *Viruses* **2023,** *15* (2), 516.
33. Selivanovitch, E.; Lafrance, B.; Douglas, T., Molecular exclusion limits for diffusion across a porous capsid. *Nat. Commun.* **2021,** *12* (1), 2309.
34. Brasch, M.; Putri, R. M.; de Ruiter, M. V.; Luque, D.; Koay, M. S. T.; Caston, J. R.; Cornelissen, J., Assembling Enzymatic Cascade Pathways inside Virus-Based Nanocages Using Dual-Tasking Nucleic Acid Tags. *J. Am. Chem. Soc.* **2017,** *139* (4), 1512-1519.
35. Wang, Y.; Uchida, M.; Waghwani, H. K.; Douglas, T., Synthetic Virus-like Particles for Glutathione Biosynthesis. *ACS Synth. Biol.* **2020,** *9* (12), 3298-3310.
36. Patterson, D. P.; Schwarz, B.; Waters, R. S.; Gedeon, T.; Douglas, T., Encapsulation of an Enzyme Cascade within the Bacteriophage P22 Virus-Like Particle. *ACS Chem. Biol.* **2014,** *9* (2), 359-365.
37. Bauler, P.; Huber, G.; Leyh, T.; McCammon, J. A., Channeling by Proximity: The Catalytic Advantages of Active Site Colocalization Using Brownian Dynamics. *The Journal of Physical Chemistry Letters* **2010,** *1* (9), 1332-1335.
38. Kraj, P.; Hewagama, N. D.; Douglas, T., Diffusion and molecular partitioning in hierarchically complex virus-like particles. *Virology* **2023,** *580*, 50-60.
39. Kostiainen, M. A.; Hiekkataipale, P.; de la Torre, J. A.; Nolte, R. J. M.; Cornelissen, J., Electrostatic self-assembly of virus-polymer complexes. *J. Mater. Chem.* **2011,** *21* (7), 2112-2117.
40. Verwegen, M.; Cornelissen, J., Clustered Nanocarriers: The Effect of Size on the Clustering of CCMV Virus-Like Particles With Soft Macromolecules. *Macromol. Biosci.* **2015,** *15* (1), 98-110.

41. Chakraborti, S.; Korpi, A.; Kumar, M.; Stępień, P.; Kostiainen, M. A.; Heddle, J. G., Three-Dimensional Protein Cage Array Capable of Active Enzyme Capture and Artificial Chaperone Activity. *Nano Lett.* **2019,** *19* (6), 3918-3924.
42. Liu, Q.; Zhou, Y.; Shaukat, A.; Meng, Z.; Kyllönen, D.; Seitz, I.; Langerreiter, D.; Kuntze, K.; Priimagi, A.; Zheng, L.; Kostiainen, M. A., Optically Controlled Construction of Three-Dimensional Protein Arrays. *Angew. Chem., Int. Ed.* **2023**, e202303880.
43. Uchida, M.; McCoy, K.; Fukuto, M.; Yang, L.; Yoshimura, H.; Miettinen, H. M.; LaFrance, B.; Patterson, D. P.; Schwarz, B.; Karty, J. A.; Prevelige, P. E.; Lee, B.; Douglas, T., Modular Self-Assembly of Protein Cage Lattices for Multistep Catalysis. *ACS Nano* **2018,** *12* (2), 942-953.
44. Parent, K. N.; Deedas, C. T.; Egelman, E. H.; Casjens, S. R.; Baker, T. S.; Teschke, C. M., Stepwise molecular display utilizing icosahedral and helical complexes of phage coat and decoration proteins in the development of robust nanoscale display vehicles. *Biomaterials* **2012,** *33* (22), 5628-5637.
45. McCoy, K.; Uchida, M.; Lee, B.; Douglas, T., Templated Assembly of a Functional Ordered Protein Macromolecular Framework from P22 Virus-like Particles. *Acs Nano* **2018,** *12* (4), 3541-3550.
46. Schwarz, B.; Madden, P.; Avera, J.; Gordon, B.; Larson, K.; Miettinen, H. M.; Uchida, M.; LaFrance, B.; Basu, G.; Rynda-Apple, A.; Douglas, T., Symmetry Controlled, Genetic Presentation of Bioactive Proteins on the P22 Virus-like Particle Using an External Decoration Protein. *ACS Nano* **2015,** *9* (9), 9134-9147.
47. Uchida, M.; Brunk, N. E.; Hewagama, N. D.; Lee, B.; Prevelige, P. E.; Jadhao, V.; Douglas, T., Multilayered Ordered Protein Arrays Self-Assembled from a Mixed Population of Virus-like Particles. *ACS Nano* **2022,** *16* (5), 7662-7673.
48. Selivanovitch, E.; Uchida, M.; Lee, B.; Douglas, T., Substrate Partitioning into Protein Macromolecular Frameworks for Enhanced Catalytic Turnover. *ACS Nano* **2021**, 15687–15699.
49. Kraj, P.; Selivanovitch, E.; Lee, B.; Douglas, T., Polymer Coatings on Virus-like Particle Nanoreactors at Low Ionic Strength—Charge Reversal and Substrate Access. *Biomacromolecules* **2021,** *22* (5), 2107-2118.
50. Lang, X.; Hong, X.; Baker, C. A.; Otto, T. C.; Wheeldon, I., Molecular binding scaffolds increase local substrate concentration enhancing the enzymatic hydrolysis of VX nerve agent. *Biotechnol. Bioeng.* **2020,** *117* (7), 1970-1978.
51. Machielsen, R.; Uria, A. R.; Kengen, S. W. M.; Van Der Oost, J., Production and Characterization of a Thermostable Alcohol Dehydrogenase That Belongs to the Aldo-Keto Reductase Superfamily. *Appl. Environ. Microbiol.* **2006,** *72* (1), 233-238.
52. Uchida, M.; LaFrance, B.; Broomell, C. C.; Prevelige, P. E.; Douglas, T., Higher Order Assembly of Virus-like Particles (VLPs) Mediated by Multi-valent Protein Linkers. *Small* **2015,** *11* (13), 1562-1570.
53. Brunk, N. E.; Uchida, M.; Lee, B.; Fukuto, M.; Yang, L.; Douglas, T.; Jadhao, V., Linker-Mediated Assembly of Virus-Like Particles into Ordered Arrays via Electrostatic Control. *ACS Appl. Bio Mater.* **2019,** *2* (5), 2192-2201.
54. Jachimska, B.; Jasiński, T.; Warszyński, P.; Adamczyk, Z., Conformations of poly(allylamine hydrochloride) in electrolyte solutions: Experimental measurements and theoretical modeling. *Colloids Surf., A* **2010,** *355* (1-3), 7-15.
55. Llauro, A.; Luque, D.; Edwards, E.; Trus, B. L.; Avera, J.; Reguera, D.; Douglas, T.; de Pablo, P. J.; Caston, J. R., Cargo-shell and cargo-cargo couplings govern the mechanics of artificially loaded virus-derived cages. *Nanoscale* **2016,** *8* (17), 9328-9336.
56. Whitesides, G. M.; Grzybowski, B., Self-Assembly at All Scales. *Science* **2002,** *295* (5564), 2418-2421.
57. Menges, F. *Spectragryph - Optical Spectroscopy Software*, 1.2.8; 2020 http://www.effemm2.de/spectragryph/ (Accessed 2018-03-05).

Table of Contents Graphic

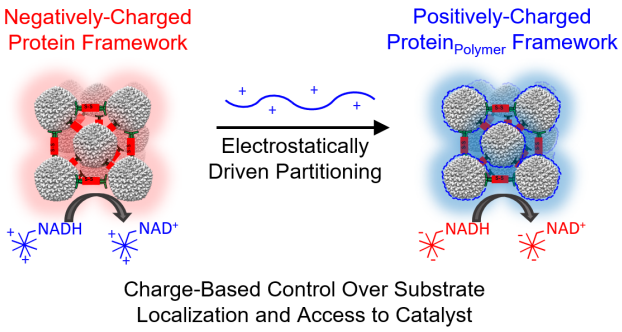

Charge-Based Control Over Substrate
Localization and Access to Catalyst